

COMPARISON OF NEAR-EUTECTIC SnPb AND SnAg SOLDER PLATING FOR WLP APPLICATIONS

Bioh Kim, Charles Sharbono, Tom Ritzdorf, and Dan Schmauch
Semitool, Inc.
Kalispell, MT, USA
bkim@semitool.com

ABSTRACT

The plating characteristics of near-eutectic SnPb and SnAg solders were compared for wafer-level packaging applications. The near-eutectic SnPb process showed a typical polarization behavior due to the close proximity of reduction potentials of the two metals. No large change in surface morphology and alloy composition was observed with varying current density. In the case of the near-eutectic SnAg deposition, silver had significantly higher reduction potential and much lower concentration than tin. This resulted in a very unique polarization behavior, showing two separate plateaus. A significant change in surface morphology and alloy composition was observed with increasing current density. A displacement reaction also occurred between the tin anode and the silver ions in the bath. With the wafer-scale deposition of SnPb solder, we observed that (i) organic components had a major impact on alloy composition and surface morphology, (ii) growth shape changed significantly with deposition conditions, and (iii) bath composition, bath aging, deposition rate, and waveform significantly impacted the probability of abnormal growths. With the wafer-scale deposition of SnAg, we observed that (i) alloy composition was a function of various deposition conditions such as current density, silver concentration, flow conditions, and pattern parameters, (ii) the surface morphology at low current densities was dendritic, and (iii) gas generation from insoluble anodes was one of the major rate-limiting factors. With both bumping processes, we achieved a similar controllability (good uniformity and repeatability of thickness and composition) at high deposition rates, and reflowed bumps had spherical shapes and smooth surfaces with no voids.

Key words : near-eutectic, SnPb, SnAg, plating, wafer-level packaging

INTRODUCTION

Mounting is a critical step in manufacturing electronic devices. As the devices are miniaturized and the circuitry becomes complicated, flip-chip (FC) technology is preferred over conventional wire bonding or tape automated bonding. The concept of wafer-level packaging (WLP) originated from efforts to combine FC technology with surface mount technology (SMT) and ball grid array (BGA) with the goal of further miniaturization and lower cost.¹ WLP is completed directly on the wafer and then singulated by dicing for the assembly in a FC fashion.

Solder bumps in WLP serve for electrical connection, mechanical support, and heat dissipation. The most practical method for producing fine-geometry bumps cost-effectively is electrodeposition. The most widely used solders are based on lead-tin alloys due to excellent plating feasibility, well-characterized solderability performance, good deposit properties, and assembly compatibility. Addition of lead to tin prevents the formation of tin whiskers, increases corrosion resistance, and lowers melting point and surface tension.

However, there is currently substantial interest in lead-free solders. The EU's Waste Electrical and Electronic Equipment (WEEE) and Restriction of Hazardous Substances (RoHS) directives propose the complete phase-out of lead in electronic products by January 2008.² Another serious concern for the upcoming technology generation is ²¹⁰Pb-created alpha-particle radiation.³ The FC interconnects should have minimal levels of alpha-particle radiation to limit soft errors in complementary metal-oxide semiconductor (CMOS) technology.

Pure tin is considered one type of lead-free material due to moderate wettability, non-toxicity, and ease of deposition. Even though some researchers showed promising results with pure tin,⁴⁻⁶ its use has been restricted due to the tendency to grow tin whiskers.^{4,7} Alloying tin with certain elements is widely believed to inhibit whisker formation. SnCu, SnAg, and SnAgCu alloys have been evaluated due to their desirable melting points, good material properties, and ability to plate and reflow.⁸⁻¹⁶ We also investigated the through-mask deposition of near-eutectic SnCu, SnAg, and SnAgCu solders for WLP. We found that the SnAg process can be more feasible for volume production than copper-containing processes (SnCu and SnAgCu) due to a longer bathlife and easier measurement and maintenance of the alloy composition.¹⁷

In this work, we performed segment-scale and wafer-scale comparisons of the plating characteristics of SnPb and SnAg solders. We (i) examined the fundamental differences between SnPb and SnAg plating (polarization behavior, surface morphology, alloy composition, and displacement reaction), (ii) examined the key deposition parameters affecting each wafer-scale plating, and (iii) compared the ability to plate and reflow at the optimized conditions.

EXPERIMENTAL METHODS

We performed segment-scale and wafer-scale tests with two types of baths (SnPb and SnAg). We used a potentiostat/galvanostat (EG&G model 263A with EG&G 270 software) for segment-scale tests such as linear sweep voltammetry, galvanostatic deposition, and potentiostatic deposition with a rotating disc electrode (RDE) or a wafer segment. Blanket wafers for segment-scale tests had the structure of Si(substrate)/SiO₂/TiN/PVD-Cu(100nm). We manufactured a modified rotating disc electrode (MRDE) to mount a wafer segment in a conventional RDE.¹⁵

200mm-diameter patterned wafers for wafer-scale tests had the structure of Si(substrate)/SiO₂/Ti or TiW/PVD-Cu/mask. Most tests were done with a BDTV1 pattern which has 130 μ m-diameter via pattern, 250 μ m pitch, 55 μ m thick resist, and 16.5% open area. We used (i) Semitool's fountain-type reactors to plate patterned wafers, (ii) a focused ion beam (FIB, FEI dual beam 820) or a scanning electron microscope (SEM, Amray model 3600 FESEM) to observe surface morphology and growth shape, (iii) an energy-dispersive spectrometer (EDS, Noran Voyager) or X-ray fluorescence spectroscopy (XRF) to examine alloy composition, and (iv) a surface metrology tool (Veeco Dektak 300-Si) to measure deposit thickness.

FUNDAMENTAL DIFFERENCES IN DEPOSITION MECHANISM

Many problems arose in SnAg solder deposition because silver had significantly higher reduction potential and much lower concentration than tin.¹⁵⁻¹⁷ This phenomenon caused several fundamental differences, including a drastic change of morphology and composition with varying current density or potential.

Polarization Behavior

Figure 1 shows a typical polarization behavior of SnPb and SnAg baths. A near-eutectic SnPb bath showed a typical polarization behavior due to the close proximity of reduction potentials of the two elements. With increasing potential, we observed the linear regime, Tafel regime, and limiting current density (LCD). A small peak in linear regime was thought to result from hydrogen gas generation. In the case of SnAg deposition, the initial curve slopes gently and then forms a plateau, corresponding to the potentials where primarily silver ions are deposited. There is no significant increase of induced current density in a wide range of potential due to the mass transfer limitation of silver ions. The deposit obtained potentiostatically at this plateau is pure silver with dendritic morphology. The curve rises sharply until it reaches the second plateau (not shown in this figure). A sharp rise after the first plateau is related to the inclusion of tin in the deposit. Therefore, SnAg alloys are obtained only when the current density is driven beyond the mass transfer limitation of silver ions. The second plateau at higher potentials is caused by the mass transfer limitation of tin ions.

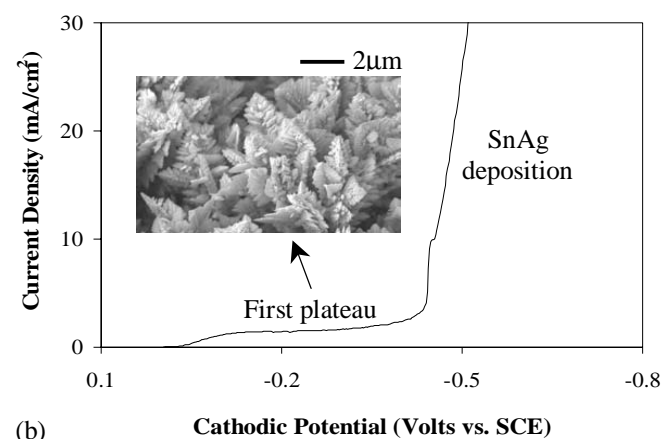
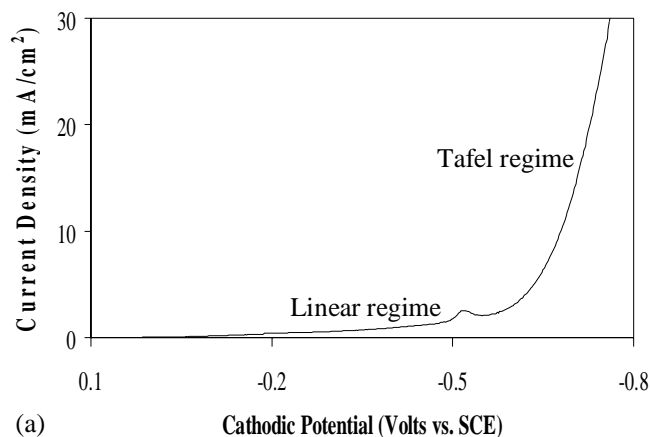


Figure 1. SnPb and SnAg polarization curves; RDE, room temperature, 1000 revolutions per minute, and scan rate 20mV/sec: (a) SnPb and (b) SnAg.

Current Density vs. Morphology and Composition

In the case of SnPb deposition, no significant change in morphology was observed with varying current density until the LCD was reached (Figure 2). This is also due to the proximity of reduction potentials of the two elements. In SnAg deposition, the morphological transition occurred through 4 stages as illustrated in Figure 3. Stage-1 dendrites result from the mass transfer limitation of silver ions. Tin becomes deposited preferentially with increasing current density, which suppresses silver dendrites (stage-2) and develops facets (stage-3). The development of facets results from the preferred orientation (or texture) of tin growth. Under mass transfer control of tin, the morphology changes again to dendrites. Unlike the SnPb alloy composition, which was very stable with current density (Figure 4(a)), the silver content in SnAg alloy dropped with increasing current density (Figure 4(b)). The content of each metal in alloy deposits is proportional to the partial current density induced by each discharge reaction. As the partial current density by silver discharge is constant after the first plateau, its fraction of the total current diminishes as the current density is increased beyond this plateau.

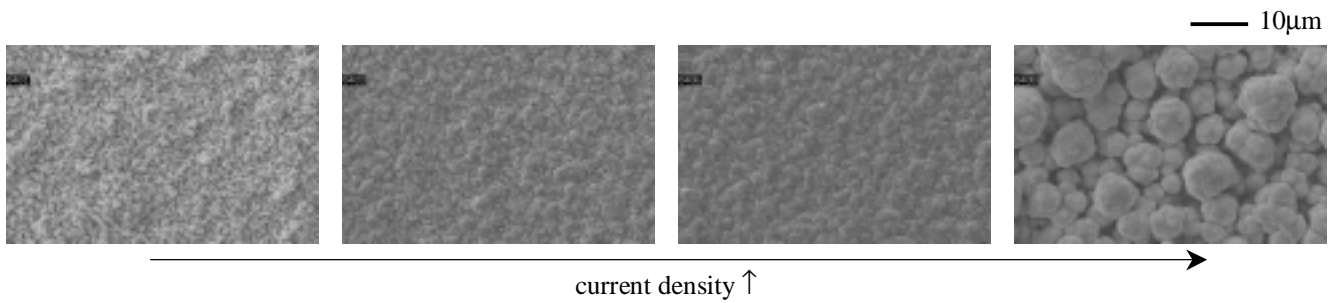


Figure 2. The morphological transition of SnPb deposits with increasing current density.

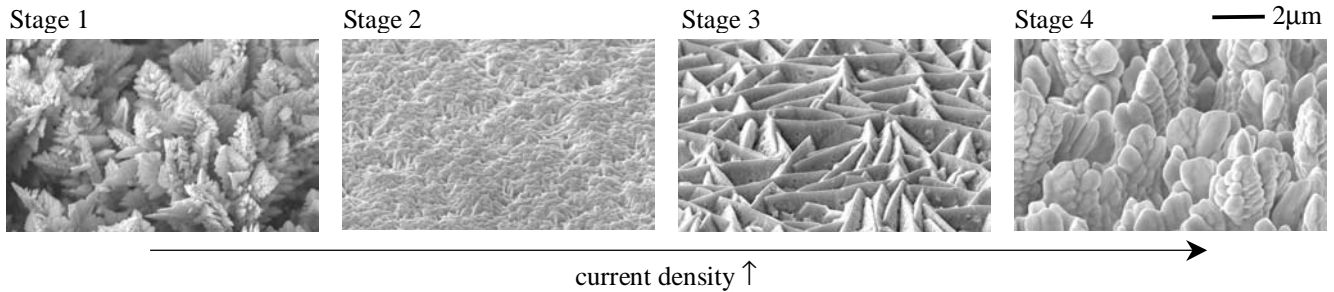


Figure 3. The morphological transition of SnAg deposits with increasing current density.

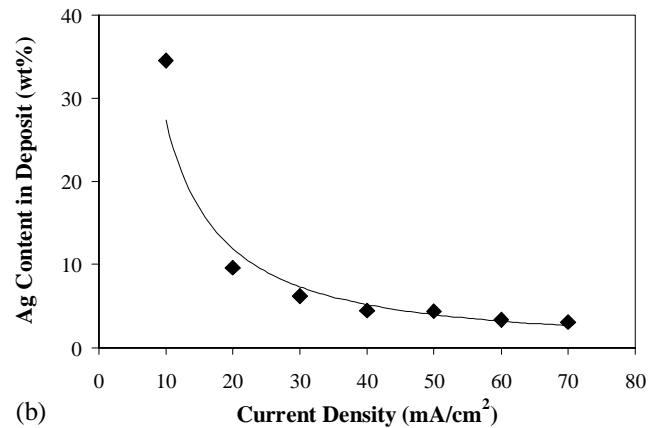
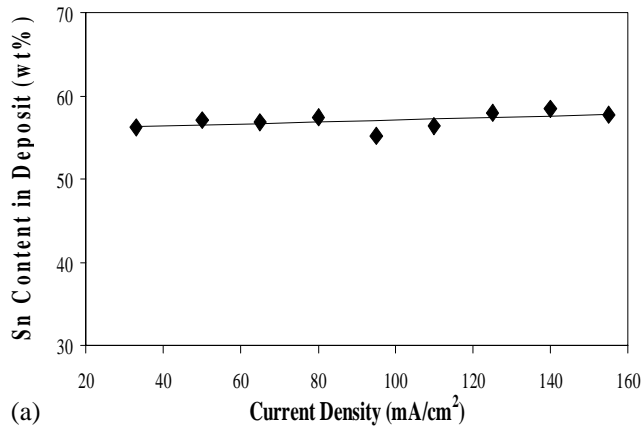


Figure 4. A variation of alloy composition with increasing current density: (a) SnPb and (b) SnAg.

Further tests showed that alloy composition was sensitive to various deposition conditions such as silver concentration, flow conditions, bath temperature, and pattern parameters (open area and resist thickness). This sensitivity arises because silver deposition is under mass transfer control.

Displacement Reaction of Tin Anodes

A difference in reduction potentials between silver and tin causes a spontaneous displacement reaction between the tin anode and the silver ions in the bath. The adhesion of silver film on the anode was poor. Figure 5 is a picture taken near the delaminated area, which shows the anode surface after the displacement reaction. We observed the significant change of tin morphology after the occurrence of this displacement reaction. SnAg alloy anodes with various silver contents could not prevent displacement reaction. When the silver content in the anode was very high, the anode behaved like an inert electrode. Consequently, in order to avoid this displacement reaction, we used inert anodes for wafer-scale SnAg plating.

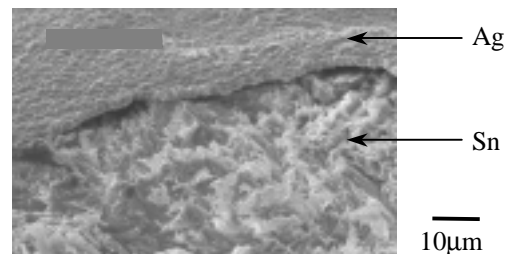


Figure 5. A change of anode surface after displacement reaction.

KEY PARAMETERS AFFECTING WAFER-SCALE SnPb DEPOSITION

Effect of Organic Additives

This plating bath contained tin ions, lead ions, methanesulfonic acid (MSA), and three organic additives; primary additive (P), secondary additive (S), and anti-oxidant (AO). Without organic components, deposits contained high tin concentration (Figure 6). P and S had a large impact on alloy composition. Without S, no stable alloy composition over current density was achieved. Figure 7 shows the impact of each organic component on the surface morphology at two different current densities. At a low current density, both P and S had a grain refining effect. At a higher current density, the impact of S on the morphology became less significant. The impacts of AO on the alloy composition and surface morphology were negligible.

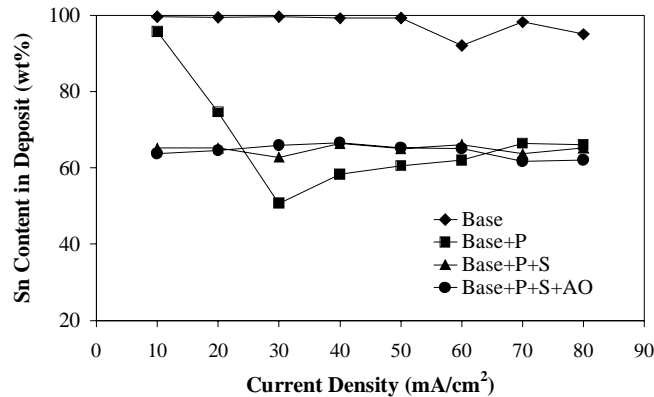


Figure 6. Effect of each organic additive on the alloy composition stability over current density.

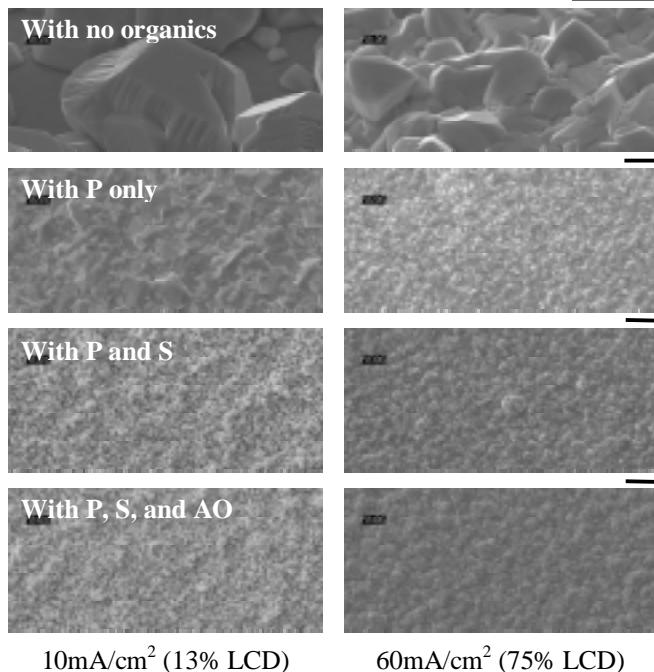


Figure 7. Effect of each organic additive on the surface morphology at two different current densities (each bar = 10 μ m).

Factors Affecting the Growth Shape of Deposits

The current distribution, mass transfer, and resultant growth shape within the via were extensively discussed by several authors.¹⁸⁻²⁶ We examined the impact of varying deposition conditions on the feature-scale growths and found that the overall growth shape of SnPb bumps were sensitive to deposition conditions.²⁷⁻²⁸ We tested the effects of wafer aging after plasma descum, deposition rate, waveform, and flow conditions. Most deposition conditions influenced the growth shape of SnPb bumps to some extent, but dominant factors varied with resist surface conditions and the fraction of limiting current density (the ratio of applied current density to LCD). We used the shape ratio (SR), which is defined as the ratio of the thickness at the via edge to the thickness at the via center, to examine the shape change with varying deposition conditions.

With aging wafers after plasma descum, SR decreased and became more affected by flow conditions. With decreasing duty cycle at a constant average current density and frequency, SR seemed to increase and growth shape became less impacted by flow conditions (wafer rotation rate, rotation direction, and solution flow rate). With increasing acid concentration, SR increased and growth shape became less impacted by flow conditions. With increasing current density, SR increased due to the increased influence of current crowding at the via edge. With further increasing current density and thus becoming closer to LCD, asymmetric deposit profiles were developed along the flow direction, and the growth shape varied significantly with flow conditions due to the increased influence of mass transfer. Figure 8 shows the impact of duty cycle on the growth shape. In both cases, the deposition rate at the via edges increased with decreasing duty cycle. Figure 9 illustrates the variation of growth shape with deposition rate. Due to wafer rotation and pattern effect, the LCD at the wafer edge was higher than that at the wafer center.

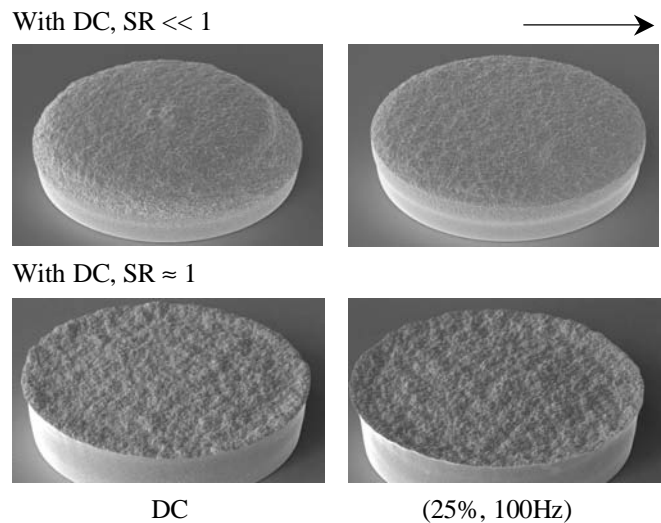
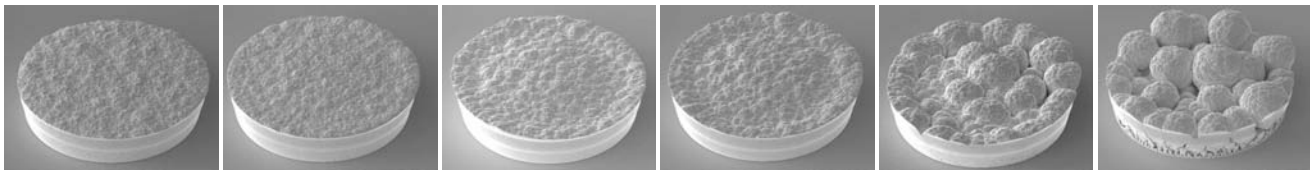
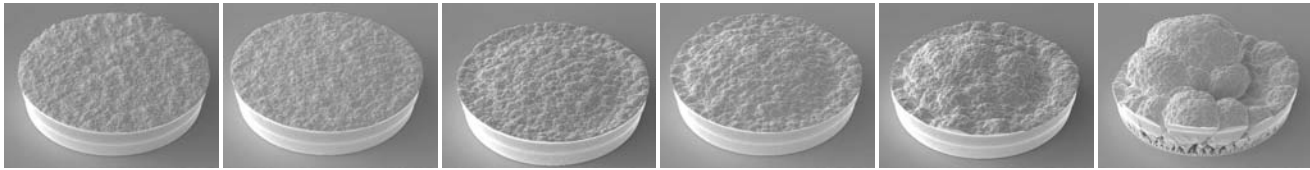


Figure 8. Effect of duty cycle on the growth shape of deposits, where the arrow indicates the average flow direction.

wafer center



wafer edge



2 μ m/min

4 μ m/min

5 μ m/min

6 μ m/min

7 μ m/min

8 μ m/min

Figure 9. Effect of deposition rate on the growth shape of deposits, where the arrow indicates the average flow direction at the wafer edge.

Factors Affecting the Probability of Abnormal Growths

Figure 10 shows the typical abnormal growth (with one or more large nodules on solder bumps) observed frequently from near-eutectic SnPb solders. The cross-section of an abnormally-grown area showed no difference in grain morphology compared with a normally-grown area. The mechanism of this type of abnormal growth is not fully understood, but some process conditions such as bath composition (organic and inorganic concentrations), deposition rate, waveform, and bath aging were experimentally proven to influence the probability of this type of abnormal growth.²⁷ The probability of abnormal growth, which is defined as the percent of abnormally grown bumps to the total number of inspected bumps, was significantly reduced with decreasing deposition rate, with decreasing duty cycle, with decreasing organic concentrations, and with increasing acid concentration. With aging the bath, the probability significantly increased.

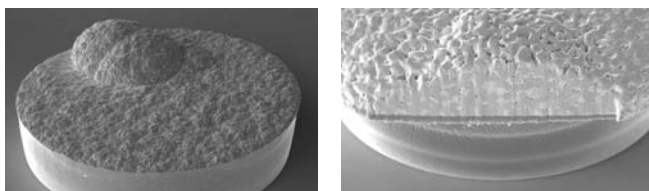


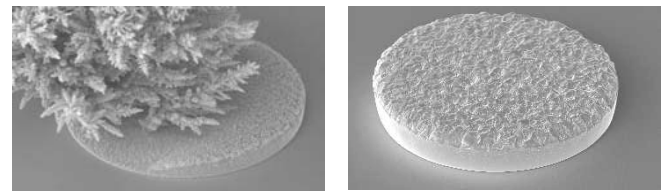
Figure 10. Abnormal growths of eutectic SnPb bumps.

KEY PARAMETERS AFFECTING WAFER-SCALE SnAg DEPOSITION

Deposition Rate vs. Surface Morphology

Due to its unique polarization behavior, very dendritic morphology was obtained at low current densities. The threshold current density which starts to generate dendritic deposits was variable depending upon pattern parameters (such as open area and resist thickness), bath composition, and resulting alloy composition. Figure 11 compares the surface morphology of bumps at two different deposition rates. In the case of SnAg plating, the optimal selection of current density (or deposition rate) was very important to prevent dendritic growth.

The maximum deposition rate was determined by bath LCD, flow conditions, pattern parameters, and the amount of gas generated from anodes (in the case of using inert anodes). In general, we can achieve the deposition rates of 1-3 μ m/min depending upon deposition conditions and pattern parameters.



0.5 μ m/min

3 μ m/min

Figure 11. Morphology comparison at two different deposition rates.

Gas Generation from Anodes vs. Deposit Quality

The amount of oxygen gas generated from anodes had a direct influence on the maximum deposition rate.²⁹ As shown in Figure 12, the gas generation starts to influence the overall growths from a certain deposition rate. This threshold deposition rate was determined by pattern parameters such as open area and resist thickness at a given deposition condition. With increasing open area and thickness, it became more difficult to achieve higher deposition rates. Non-uniform thickness, morphology, and shape were obtained from the threshold deposition rate.

Bath Composition vs. Growth Shape and Void Formation

We compared a variety of SnAg baths to achieve good growth morphology and shape with no voids.¹⁷ Those results were very sensitive to bath composition. Some baths produced very poor growth shape and shape uniformity (even within a very small area) as shown in Figure 13. These baths also caused severe voiding after reflow. This phenomenon was believed to result from the organic components in those baths. With an optimized bath, we can achieve void-free fill with various patterns. Figure 14 shows

the cross-sections of various bump structures; SnAg only, Ni/SnAg, Cu/SnAg, and Cu/Ni/SnAg.

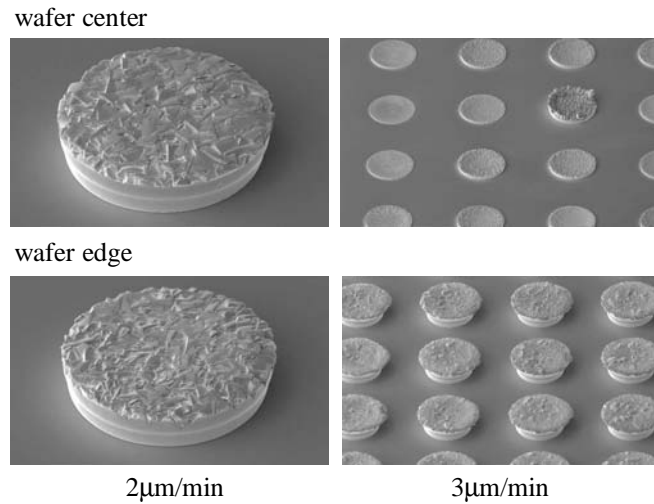


Figure 12. Effect of gas generation from anodes on the deposit quality.

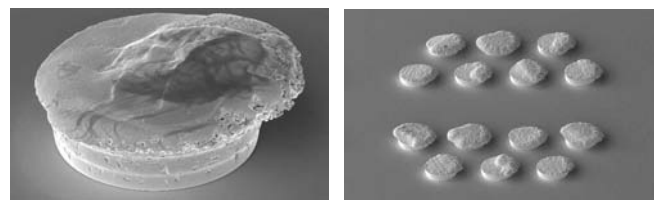


Figure 13. Poor growth shape and shape uniformity with a non-optimized bath.

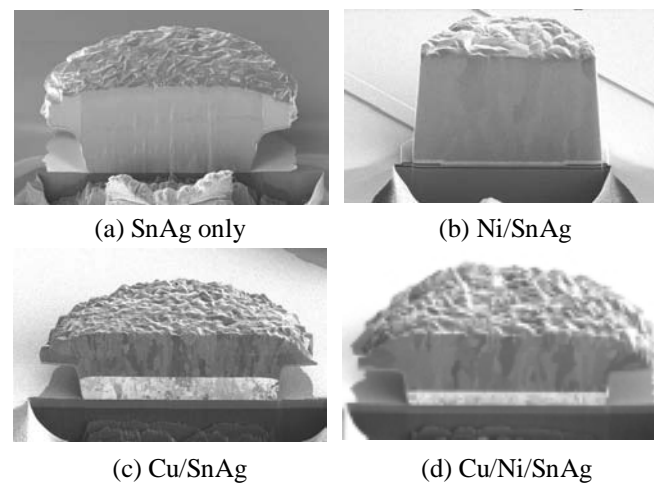


Figure 14. Cross-sections of bumps with various UBM structures and heights on TiW/Cu seed: (a) 55µm thick resist and 130µm-diameter via, (b) 100µm thick resist and 90µm-diameter via, (c) and (d) 25µm thick resist and 100µm-diameter via.

COMPARISON OF ABILITY TO PLATE AND REFLOW

We compared surface morphology, growth shape, uniformity (thickness and composition), and ability to reflow. With a BDTV1 pattern, we selected the deposition rate of 4µm/min for SnPb plating and 2µm/min for SnAg plating. The maximum achievable deposition rate of SnAg was lower than that of SnPb because gas generation from anodes impacted deposit qualities.

Figure 15 compares the growth shape and morphology of SnPb and SnAg bumps. As shown in this figure, we can achieve smooth morphology and good mushroom shape with no void formation in both cases. Reflow tests were performed with device wafers. All wafers showed spherical shapes and smooth surfaces. No significantly large voids were observed from cross-sections and X-ray transmission. Figure 16 shows reflowed bumps.

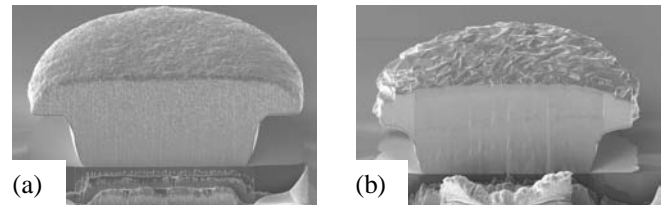


Figure 15. Comparison of bump shape and morphology at optimized conditions: (a) near-eutectic SnPb; 4µm/min and (b) near-eutectic SnAg; 2µm/min.

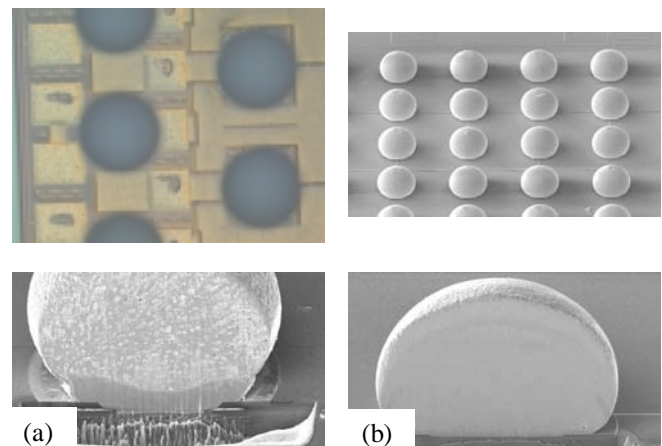


Figure 16. Reflowed bumps: (a) SnPb; 4µm/min and (b) SnAg; 2µm/min.

Figure 17 compares the repeatability of within-wafer thickness uniformity and alloy composition. The uniformity of thickness and composition was within the specifications. We achieved within-wafer thickness uniformity $<\pm 10\%$ and alloy composition $<\pm 3\text{wt}\%$ with SnPb plating and obtained within-wafer thickness uniformity $<\pm 10\%$ and alloy composition $<\pm 0.5\text{wt}\%$ with SnAg plating.

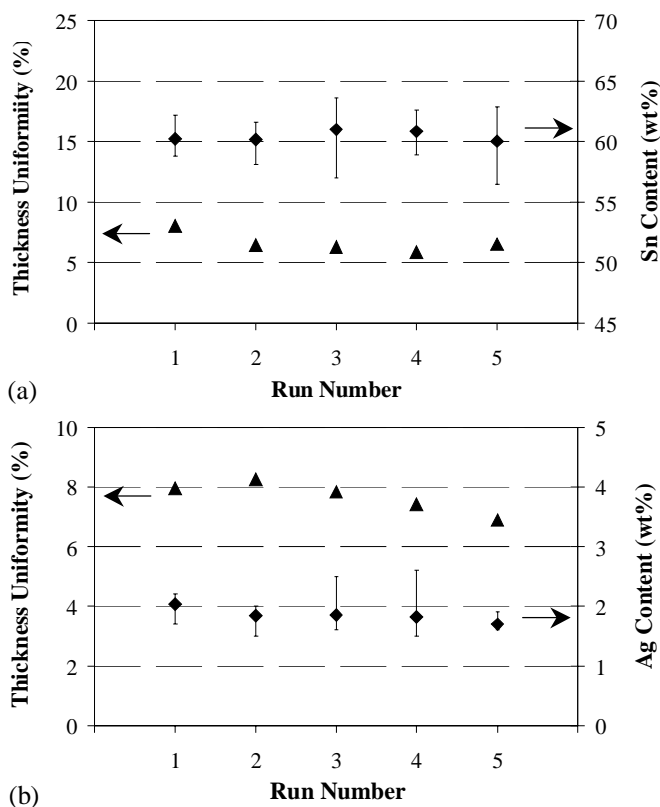


Figure 17. Comparison of thickness and composition uniformity at optimized conditions: (a) near-eutectic SnPb; 4µm/min and (b) near-eutectic SnAg; 2µm/min.

CONCLUSIONS

The plating characteristics of near-eutectic SnPb and SnAg solders were compared for WLP applications. The near-eutectic SnPb process showed a typical polarization behavior due to the close proximity of reduction potentials of the two metals. No large change in surface morphology and alloy composition was observed with varying current density. In the case of the near-eutectic SnAg deposition, silver had significantly higher reduction potential and much lower concentration than tin. This resulted in a very unique polarization behavior, showing two separate plateaus. A significant change in surface morphology and alloy composition was observed with increasing current density. An undesirable displacement reaction occurred between the tin anode and the silver ions in the bath, which led to the use of inert anodes for SnAg deposition.

With the wafer-scale deposition of SnPb solder, we observed that (i) organic additives (primary and secondary additives) had a major impact on alloy composition and surface morphology, (ii) growth shape was very sensitive to deposition conditions, and (iii) bath composition, bath aging, deposition rate, and waveform significantly impacted the probability of abnormal growths. With the wafer-scale deposition of SnAg, we observed that (i) alloy composition was a function of various factors such as current density, silver concentration, flow conditions, bath temperature, and pattern parameters, (ii) the surface morphology at low

current densities was very dendritic, and (iii) gas generation from insoluble anode was one of the major rate-limiting factors. With both bumping processes, we achieved good uniformity and repeatability of thickness and composition at high deposition rates, and reflown bumps had spherical shapes and smooth surfaces with no large voids.

REFERENCES

1. M. Töpper and H. Reichl, Future Fab International, Issue 11, Section 9 (2001).
2. <http://164.36.164.20/sustainability/weee/index.htm>.
3. J. F. Ziegler, IBM J. Res. Dev., 40 (1), p. 3 (1996).
4. R. Schetty, Plating & Surface Finishing, March, p. 48 (2003).
5. A. Sriyarunya and R. Schetty, "Lead-free Plating for Semiconductor Devices – Production Qualification & Implementation", AESF SUR/FIN Conference (2003).
6. R. Bidin, R. Tagapulot, C. N. D. Lao, and R. Manalac, Advanced Packaging, April, p. 29 (2001).
7. B. Z. Lee and D. N. Lee, Acta Mater., 46 (10), p. 3701 (1998).
8. O. Khaselev, I. S. Zavarine, A. Vysotskaya, and Y. Zhang, "Electrodeposition of Tin Alloys Toward Lead-free Solder", AESF SUR/FIN Conference (2001).
9. J. Swanson and Y. Zhang, Plating & Surface Finishing, January, p. 14 (2002).
10. C. Tanner, "Lead-free Soldering Reliability Characterization Efforts", Proceedings of the International Workshop on Lead- and Halide-free Electronics, Semicon Europa (2000).
11. K. Nimmo, "Lead-free Solder Alloy Candidates and Patent Issues", Proceedings of the International Workshop on Lead- and Halide-free Electronics, Semicon Europa (2000).
12. H. Shimokawa, T. Soga, T. Nakatsuka, and K. Serizawa, International Conference on Electronics Packaging (ICEP) Proceedings, p. 78 (2001).
13. W. Yang, L. E. Felton, and R. W. Messler, Jr., J. Electro. Mater., 24, p. 1465 (1995).
14. T. Kobayashi, J. Tanaka, S. Hayashi, T. Takashima, and T. Narita, International Conference on Electronics Packaging (ICEP) Proceedings, p. 66 (2001).
15. B. Kim and T. Ritzdorf, J. Electrochem. Soc., 150 (2), p. C53 (2003).
16. B. Kim and T. Ritzdorf, J. Electrochem. Soc., 150 (9), p. C577 (2003).
17. B. Kim, T. Ritzdorf, D. Schmauch, and P. Sibley, "Through-mask Electrodeposition of Leadfree Solders for Wafer-level Packaging Applications", Proceedings of International Wafer Level Packaging Congress (SMTA-IWLPC) (2004).
18. J. O. Dukovic, IBM J. Res. Dev., 37 (2), p. 125 (1993).
19. K. Kondo, K. Fukui, K. Uno, and K. Shinohara, J. Electrochem. Soc., 143 (6), p. 1880 (1996).
20. K. Kondo, K. Fukui, M. Yokoyama, and K. Shinohara, J. Electrochem. Soc., 144 (2), p. 466 (1997).
21. K. Kondo and K. Fukui, J. Electrochem. Soc., 145 (3), p. 840 (1998).

22. K. Kondo and K. Fukui, *J. Electrochem. Soc.*, 145 (9), p. 3007 (1998).
23. M. Georgiadou, R. Mohr, and R. C. Alkire, *J. Electrochem. Soc.*, 147 (8), p. 3021 (2000).
24. K. Hayashi, K. Fukui, Z. Tanaka, and K. Kondo, *J. Electrochem. Soc.*, 148 (3), p. C145 (2001).
25. V. R. Subramanian and R. E. White, *J. Electrochem. Soc.*, 149 (10), p. C498 (2002).
26. P. McHugh, G. Wilson, and M. Roberts, “*Electrochemical Deposition Modeling Comparison between Blanket and Selective, Through-mask Pattern Applications*”, *AIChE Annual Meeting Proceedings*, paper number : 190h (2003).
27. B. Kim and T. Ritzdorf, *J. Electrochem. Soc.*, 151 (5), p. C342 (2004).
28. B. Kim, T. Ritzdorf, C. Sharbono, and G. Saveskie, “*Effects of Deposition Conditions on the Feature-scale Growths of Through-mask Deposited Metals*”, 206th *ECS Meeting* (2004).
29. B. Kim, B. Batz, and T. Ritzdorf, “*Factors Limiting the Electrodeposition Rate of Various Bumps for Flip-Chip Interconnects*”, *Proceedings of 1st IMAPS-Device Packaging Conference* (2005).